Current Biology 23, 1939–1944, October 7, 2013 ©2013 Elsevier Ltd All rights reserved http://dx.doi.org/10.1016/j.cub.2013.07.083

Report

A 3D Map of the Yeast Kinetochore Reveals the Presence of Core and Accessory Centromere-Specific Histone

Julian Haase,[1,4] Prashant K. Mishra,[3,4] Andrew Stephens,[1] Rachel Haggerty,[1] Cory Quammen,[2] Russell M. Taylor II,[2] Elaine Yeh,[1] Munira A. Basrai,[3,5,*] and Kerry Bloom[1,5,*]
[1]Department of Biology
[2]Department of Computer Science
University of North Carolina at Chapel Hill, Chapel Hill, NC 27599-3280, USA
[3]Genetics Branch, Center for Cancer Research, National Cancer Institute, NIH, Bethesda, MD 20892, USA

Summary

The budding yeast kinetochore is ~68 nm in length with a diameter slightly larger than a 25 nm microtubule [1]. The kinetochores from the 16 chromosomes are organized in a stereotypic cluster encircling central spindle microtubules. Quantitative analysis of the inner kinetochore cluster (Cse4, COMA) reveals structural features not apparent in singly attached kinetochores. The cluster of Cse4-containing kinetochores is physically larger perpendicular to the spindle axis relative to the cluster of Ndc80 molecules [2]. If there was a single Cse4 (molecule or nucleosome) at the kinetochore attached to each microtubule plus end, the cluster of Cse4 would appear geometrically identical to Ndc80. Thus, the structure of the inner kinetochore at the surface of the chromosomes remains unsolved. We have used point fluorescence microscopy and statistical probability maps [2] to deduce the two-dimensional mean position of representative components of the yeast kinetochore relative to the mitotic spindle in metaphase. Comparison of the experimental images to three-dimensional architectures from convolution of mathematical models reveals a pool of Cse4 radially displaced from Cse4 at the kinetochore and kinetochore microtubule plus ends. The pool of displaced Cse4 can be experimentally depleted in mRNA processing *pat1*Δ or *xrn1*Δ mutants. The peripheral Cse4 molecules do not template outer kinetochore components. This study suggests an inner kinetochore plate at the centromere-microtubule interface in budding yeast and yields information on the number of Ndc80 molecules at the microtubule attachment site.

Results

Nanometer Localization Accuracy of Kinetochore Proteins in Two Dimensions Reveals Structural Features of Inner versus Outer Components

The kinetochores from each sister chromatid biorient to opposite spindle poles and can be visualized as two distinct spots along the mitotic spindle in budding yeast. Each fluorescent spot contains kinetochores from all 16 yeast chromosomes, with one microtubule per kinetochore. To determine the spatial geometry of GFP-tagged kinetochore proteins, we compiled a two-dimensional density map of their distribution from a population of metaphase cells (Figure 1 and Figure S1 available online). The mean spatial distributions of N-Ndc80, C-Ask1, C-Nuf2, C-Spc24, C-Ame1 (COMA), N-Cse4, and C-Cep3 (centromere [CEN] DNA binding factor CBF3) are shown in Figure 1. At metaphase, the N-terminal microtubule binding domain of Ndc80 is 68 nm from the N terminus of the centromere-specific histone H3 variant, Cse4p (Figure 1B). The density maps recapitulate the axial distances determined previously by pairwise centroid mapping [1]. The mean distance of the cluster of kinetochores from each spindle pole decreases about 160 nm from metaphase to late anaphase (Figure 1B). The metaphase and anaphase measurements in Figure 1B are lined up relative to the N terminus of Ndc80 to visualize the changes that occur in contraction and expansion of subregions within the kinetochore and the centromere binding factor Cep3 (Figure 1C).

The statistical probability maps extend information obtained from centroid measurements to a second dimension perpendicular to the spindle axis. Ndc80 is restricted to 94 nm versus the 181 nm spread exhibited by Cse4 (Figures 2 and S2). The increase in spread of Cse4 as well as Ame1 (COMA complex; Figure 2) along the y axis is inconsistent with models placing the centromere nucleosome exclusively at the plus end of the kinetochore microtubule.

To understand the distribution of Cse4, we have used model convolution of a mathematical simulation of the yeast spindle [3]. The model is based on stochastic growth and shortening dynamics of spindle and kinetochore microtubules and an electron microscopy- and tomographic- based geometric representation of a cylindrical spindle 250 nm in diameter. The kinetochore microtubule plus ends approximate the position of Ndc80 from the spindle pole body (Figure 2; model and Ndc80). Fluorophores placed at the microtubule plus ends were used to simulate the distribution of Ndc80. Simulated image stacks were convolved, and a statistical probability map was generated (Figure 2; Experimental Procedures; Supplemental Experimental Procedures). The width distribution (y axis) of simulated images is 90 ± 80 nm (Figure 2; Experimental Procedures), comparable to experimental measurements (Figure 2; Ndc80; 95 ± 95 nm). Line scans through Ndc80 images and simulations are indicative of highly similar distributions of the two populations (Figure S2). Unlike Ndc80, the model fails to predict the spread of Cse4 (181 ± 155 nm) and COMA (153 ± 138 nm) perpendicular to the spindle axis (Figure 2; line scans in Figure S2).

Genetic Requirements for Expansion of the Inner Kinetochore at the Chromosome Surface

To identify the genetic basis for the distribution of Cse4, we screened several mutants involved in centromere function. A reduction in the radial distribution of Cse4 would transform the appearance of Cse4 in single cells from an anisotropic structure, as described by Haase et al. [2], to an isotropic diffraction spot on the spindle axis (Figure 3, inset). Mutants in two genes, protein associated with topoisomerase (Pat1) and Xrn1, altered the appearance of Cse4 (Figure 3). Line

[4]These authors contributed equally to this work and are co-first authors
[5]These authors contributed equally to this work and are co-senior authors
*Correspondence: basraim@mail.nih.gov (M.A.B.), kerry_bloom@unc.edu (K.B.)

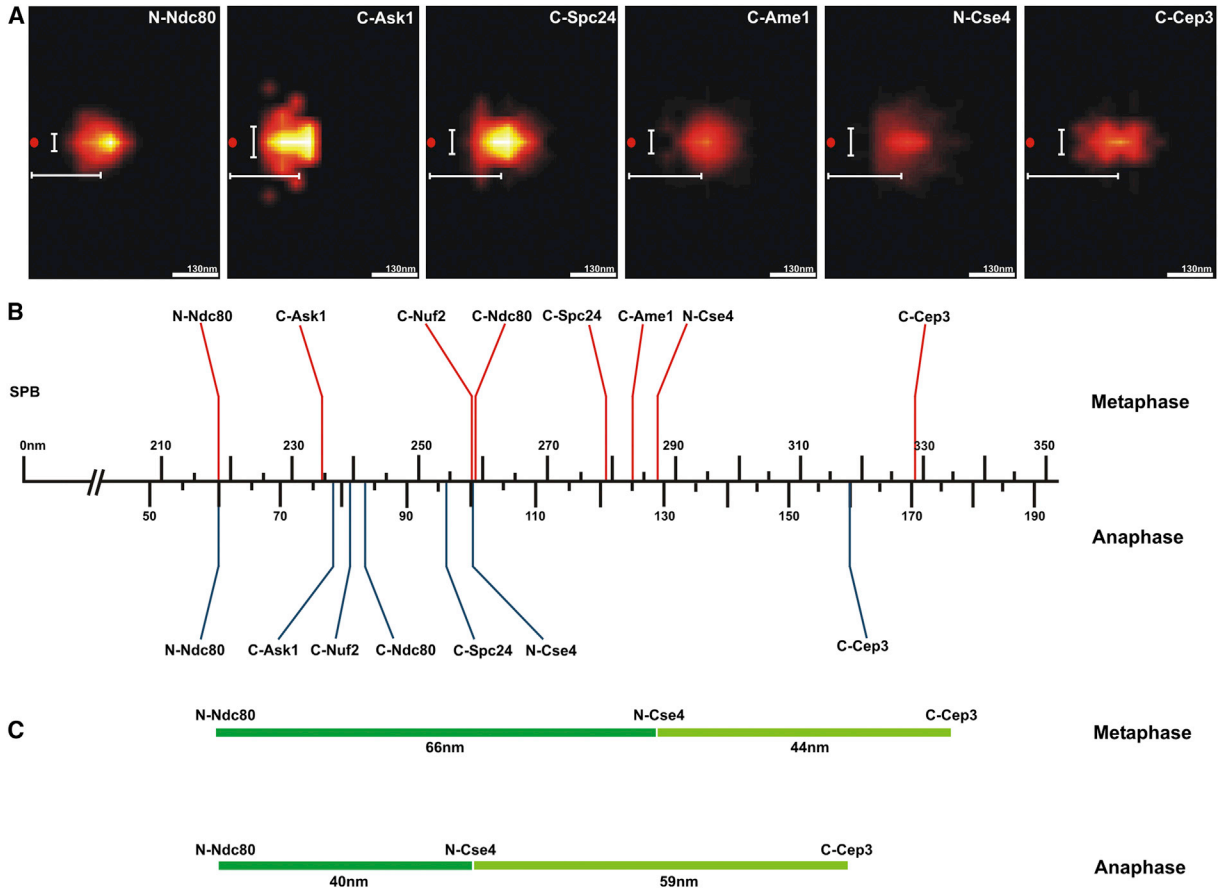

Figure 1. Two-Dimensional Mapping of Representative Kinetochore Proteins and Pericentric Chromatin

(A) The peak intensities (pixel) of clustered kinetochore foci (Ndc80, Ask1, Nuf2, Spc24, Ame1, Cse4, and Cep3) were determined and the coordinates of the brightest pixel of each spot were plotted relative to the spindle pole body (SPB), (0,0) nm. The horizontal bar (white) below the position of each density map indicates the average distance along the x axis from the spindle pole (SPB red spot). The vertical bar (white) left of the density map indicates the average displacement along the y axis.

(B) The average distance from density maps for representative proteins was determined and plotted relative to the spindle pole body (n = 1,064 for Ndc80, n = 1,032 Cse4, and n = ~100 for others). Above the axis are distance measurements from metaphase cells (red; adapted from Figure S4 in [2]). Below the axis are distance measurements taken from anaphase cells (blue). The kinetochore is approximately 68 nm in length from the N terminus of microtubule binding protein Ndc80p to the N terminus of the centromere-specific histone H3 variant, Cse4. The density maps recapitulate the linear distances determined by pairwise centroid mapping (see Figure S4 in [2]) and allow us to map the average position of components that are larger than diffraction-limited spots.

(C) The change in kinetochore length (dark green) and centromere proximal chromatin (Cse4-Cep3; light green) from metaphase (top) to anaphase (bottom).

See also Figure S1 for detailed methodology, Table S1 for assessment of localization accuracy, and Table S2 for accuracy of brightest pixel versus centroid of Gaussian fits.

scans through the cluster of Cse4 provide a quantitative measure of the spread perpendicular to the spindle axis (height in y axis of Figure 3A). Cse4 spans 660 nm in wild-type cells. In contrast, the spread of Cse4 along the y axis is reduced to 570 nm in *pat1*Δ and 583 nm in *xrn1*Δ. The aspect ratio of the Cse4 cluster (height in y axis/width in x axis) is 1.23 in wild-type versus 1.06 in *pat1*Δ and *xrn1*Δ. Pat1 is a multifunctional protein that regulates the chromatin structure and topological state of centromere [3], as well as providing a scaffold for mRNA decapping [4]. Pat1 is found in cytoplasmic P-bodies, where it functions with a number of components, including Xrn1, the primary cytoplasmic 5′ to 3′ exonuclease for mRNA degradation [4, 5].

The two-dimensional statistical analysis of Cse4 in *pat1*Δ confirms and extends the single-cell analysis. Cse4 in wild-type and *pat1*Δ cells are within 5 nm relative to the spindle pole body (wild-type [WT] 286 ± 120 nm; *pat1*Δ 281 ± 74nm; Figure 2). The spread of Cse4 perpendicular to the spindle (y axis) is reduced almost 2-fold in *pat1*Δ cells (WT, 181 ± 155 nm; *pat1*Δ, 108 ± 102 nm; Figure 2). The Pat1-independent pool of Cse4 is more comparable to Ndc80 (95 nm) and simulated microtubule plus ends (90 nm; Figure 2). The y axis distribution of Ndc80 remained unchanged in the *pat1*Δ mutant (Figure 3A).These data indicate that Cse4 and therefore the centromere nucleosome is focused exclusively at the microtubule plus end in the absence of Pat1. Interestingly, the COMA complex (Ame1) remains anisotropic in the absence of Pat1 (Figure 3A). Thus, the redistribution of Cse4 is not a global change in inner kinetochore structure.

The Number of Cse4 Molecules Is Reduced in pat1Δ Mutants

The expansion of Cse4 at the surface of the chromosome in wild-type cells could be accounted for by additional molecules [6, 7] or a single nucleosome that exhibits more freedom of movement relative to outer kinetochore components. To

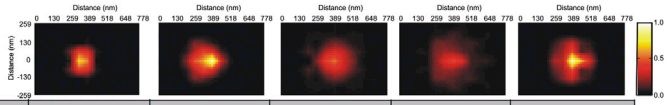

	Model	Ndc80	Ame1	Cse4	Cse4 pat1Δ
Distance from pole (nm):	219.12	219.25	283.69	286.85	281.08
SD	49.36	76.04	105.49	120.90	74.74
Width across spindle (nm):	90.48	94.61	153.39	180.92	108.86
SD	79.98	94.64	138.08	155.90	102.66

Figure 2. Model Convolution Recapitulates Ndc80 at Microtubule Plus Ends but Not Chromatin-Bound Cse4

(Top) Statistical probability maps from experimental and simulated images (model, Ndc80, Ame1, Cse4, Cse4 *pat1*Δ). (Bottom) Statistical analysis of images. Distance from the pole is the mean distance. The width across the spindle is determined by summing the average distance above and below the spindle axis. As shown in Figure S1, the density maps are mirrored from one quadrant. Experimental density maps for Ndc80 and Cse4 are generated from >1,000 images. Simulated density maps (model) and experimental Ame1 and Cse4pat1Δ are generated from >200 images. See also Figures S1 and S2 for line scans through the respective probability maps and Table S1.

distinguish these possibilities, we measured the integrated Cse4-GFP fluorescence intensity in bioriented kinetochore clusters in wild-type and *pat1*Δ cells [7].The concentration of the cluster of Cse4 in metaphase is reduced 40% in *pat1*Δ and *xrn1*Δ mutants (Figure 3B). This reduction represents the loss on average of 2–2.5 molecules, leaving ~3 Cse4 molecules at the kinetochore. Accordingly, chromatin immunoprecipitation experiments showed an ~60% reduction in *CEN*-associated Cse4 in *pat1*Δ (0.72% at CEN1, 0.80% at CEN3, and 0.53% at CEN5) versus wild-type (2.02% at CEN1, 1.92% at CEN3, and 1.59% at CEN5; Figure S3A). Thus, Pat1 and Xrn1 are required for the full complement of Cse4 at the yeast kinetochore, and further, there is an excess of Cse4 molecules beyond that needed for proper attachment. The reduction in Cse4 fluorescence in *pat1*Δ and *xrn1*Δ mutants excludes the possibility of a single Cse4 in each of the 16 kinetochores clustered around the spindle microtubules [8].

Accessory Cse4 Molecules Do Not Nucleate Kinetochore Assembly

The dependence of Cse4 on Pat1 and Xrn1 provides the opportunity to determine whether excess Cse4 nucleate the assembly of outer kinetochore components. The quantity of Ndc80 and Ame1 (COMA) remains within 85% of their wild-type level in the absence of Pat1 (Figure 3B). The number of Ndc80 molecules per core Cse4 is ~17, consistent with measurements in chicken DT-40 (~19; [7, 9]) and HeLa (~13; A. Suzuki and E.D. Salmon, personal communication) cells. Accessory Cse4 molecules do not contribute to the assembly of outer kinetochore components.

Loss of Peripheral Cse4 Results in Cell-Cycle Delay

pat1Δ mutant cells lacking peripheral Cse4 exhibit a delay of about 40 min in cell-cycle progression and Pds1 degradation (Figures S3B and S3C). The bulk of Pat1 is present in dispersed cytoplasmic foci (P-bodies; [10]; Pat1-GFP; Figure S4), but nuclear accumulation has been reported in lsm1Δ cells [10]. Quantitative RT-PCR reveals that levels of Cse4 mRNA are unchanged in wild-type versus pat1Δ mutants (Figure S3D). This is consistent with whole-cell Cse4 protein fluorescence measurements in wild-type, *pat1*Δ, and *xrn1*Δ mutants (Figure 3B). Therefore, it is unlikely that Pat1 function at centromere proceeds through regulation of Cse4 mRNA [3].

Model Convolution to Estimate the Position of Accessory Cse4 Molecules

If the additional Cse4 molecules are not at kinetochore plus ends, it should be possible to deduce their spatial position using model convolution to match experimental observations. Toward this end, we generated the distribution of kinetochore microtubule lengths (along the x axis) derived from the mathematical model that best fits Ndc80 (Figure 2). Instead of mapping these lengths directly onto kinetochore microtubules, we allow the fluorophores to explore a larger area perpendicular to the spindle axis (see blue probability bubble in Figure 4). If all Cse4 molecules explore positions distant from the microtubule plus end, the model fails to match experimental images (data not shown). The geometry that best matches experimental images is a single nucleosome at the kinetochore microtubule attachment site and three to four radially displaced molecules (Figure 4). This result is visually represented in Figure 4, where we have clustered 16 kinetochores and their individual probability bubbles around the central spindle (Figure 4; 1X and 16X). Note that the inner kinetochore (blue) appears anisotropic relative to outer components (Ndc80; orange rods at microtubule plus ends), with dimensions that match experimental (Figure 2). The radial displacement from the microtubule plus end required to match anisotropy and the statistical probability maps for wild-type Cse4 is ~250 nm. Cse4 in the pat1Δ mutant appears dimmer and isotropic in experimental (Figures 2 and 3) and matches the distribution of Ndc80 and microtubule plus ends (16X *pat1*Δ; Figure 4). Thus, in wild-type cells, there is a Cse4 core at microtubule plus ends, whereas additional Cse4 molecules as well as COMA (Ame1) form a disc on the surface of the pericentromere at the interface of the microtubule attachment site. The diameter of the disc is comparable to the diameter of the cohesin barrel (Figure 4) [11].

Discussion

The organization of the inner kinetochore at the chromosome interface is poorly understood. The inner kinetochore is distinct from the outer kinetochore, as determined by the oblate geometry of Cse4 and the COMA complex (Ame1; Figure 2B) [2]. This geometry has not been predicted by either in vivo [1] or in vitro [14] structural models of the kinetochore. By reducing the number of Cse4 molecules in the cluster of 16 kinetochores via deletion of Pat1 and Xrn1, we define a core Cse4 complex of approximately two to three molecules/kinetochore in geometric alignment with the outer kinetochore. The peripheral Cse4 molecules are displaced laterally from the kinetochore hub at microtubule plus ends. Using mathematical models and model convolution to assess geometries that match experimental observations [12, 15], we find the accessory molecules most likely reside on the surface of the chromosome and are radially confined by the dimension of the cohesin barrel (~500 nm diameter; Figure 4; wild-type). The

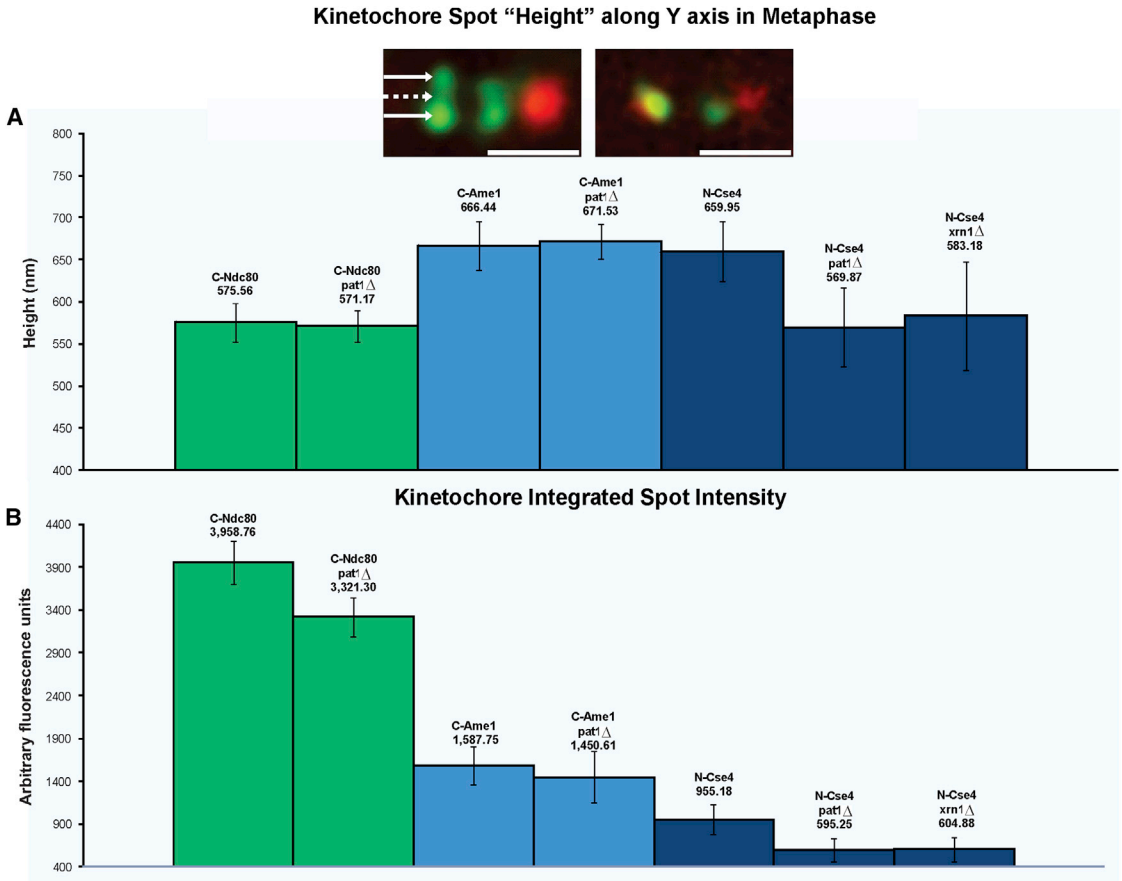

Figure 3. Quantitative Fluorescence and Kinetochore Anisotropy

(A) The height of the cluster of kinetochore proteins was determined from line scans (perpendicular to the spindle axis) through the protein cluster. The height was determined from the full-width full-maximum of the Gaussian distribution. Foci of Cse4-GFP extend perpendicular to the spindle axis (660 nm y axis) compared to outer kinetochore Ndc80-GFP (576 nm y axis). The aspect ratio (height/width) for Cse4 is 1.23 versus 1.07 of Ndc80. The cluster of Cse4 is no longer anisotropic in *pat1*Δ or *xrn1*Δ mutants (*pat1*Δ 570 nm; *xrn1*Δ 583 nm; aspect ratio width/height = 1.06). Inset, deconvolution microscopy of Cse4 in wild-type and *pat1*Δ mutants. Left, Cse4 (green) appears punctuate upon deconvolution. Arrows mark peaks of bright spots (outer arrows) and dim center (middle dashed arrow). The average outer peak intensity is 352 ± 64 arbitrary units. The average center intensity is 146 ± 35 arbitrary units. The ratio of outer/inner intensity is 2.4. Right, Cse4 in *pat1*Δ (green) appears as a single spot coincident with the spindle axis (spindle pole body, red). The scale bars represent 1 μm.

(B) The fluorescence intensity of Cse4, Ndc80, and Ame1 in wild-type, *pat1*Δ, or *xrn1*Δ metaphase cells. There is a 40% decrease in Cse4 at the centromere in the absence of Pat1 and Xrn1. There is 15% decrease of Ndc80 and 10% decrease of Ame1. Whole-cell Cse4 fluorescence is not reduced in mutant cells (WT 24,355 arbitrary units [a.u.]; *pat1*Δ 32,516 a.u.; *xrn1*Δ 33,654 a.u.). See Figure S3A for chromatin immunoprecipitation of centromeric Cse4 in the absence of *pat1*Δ. See also Figures S3 and S4.

inner kinetochore represents the molecular interface between chromatin and spindle microtubules. This arrangement indicates that Cse4 and other inner kinetochore components, including COMA, constitute a chromatin plate of the inner kinetochore, much like that observed in the trilaminar structure at the chromosome surface of a mammalian kinetochore [16].

The centromere-specific nucleosome represents 1/5,000 of total nucleosomes. The apparent confinement of excess Cse4 molecules to the vicinity of the kinetochore allows for rapid incorporation of Cse4 in the event of eviction at the centromere. The nucleosomes in the pericentric region are dynamic [17], with the balance between eviction and insertion modulated by chromatin remodelers, including at least *STH1/NPS1* and *ISW2*. Whereas the centromere histone is stable in metaphase [18], the loss of a single nucleosome (1/16) would be catastrophic and below the sensitivity of Pearson et al. [18]. The proposal that a pool of Cse4 is important for these rogue loss events is reminiscent of the abundance of Sir2 proteins at telomeres [19]. Gasser et al. [19] proposed a mechanism, known in enzymology as the Circe effect [20], in which a local ligand is enriched relative to the binding site.

These accessory molecules may or may not be incorporated into chromatin, consistent with their absence from the deep-sequencing efforts [21]. In addition, the observed variability in centromeric Cse4 protein number from strain to strain [7] is also consistent with a variable number of accessory Cse4 flanking the CEN. Finally, these accessory molecules will not be observed on single kinetochores of lagging chromosomes or dicentric chromosomes in anaphase after destruction of the cohesin barrel. We expect that only the core Cse4 molecules would be observed on lagging chromosomes or dicentric chromosomes. The proposal that a small number of molecules in a reservoir "ready for action" is not new to the field of enzymology [20]. The discovery of an inner kinetochore plate at the surface of the pericentric chromatin furthers the proposal for the yeast spindle as a model for a single mammalian kinetochore.

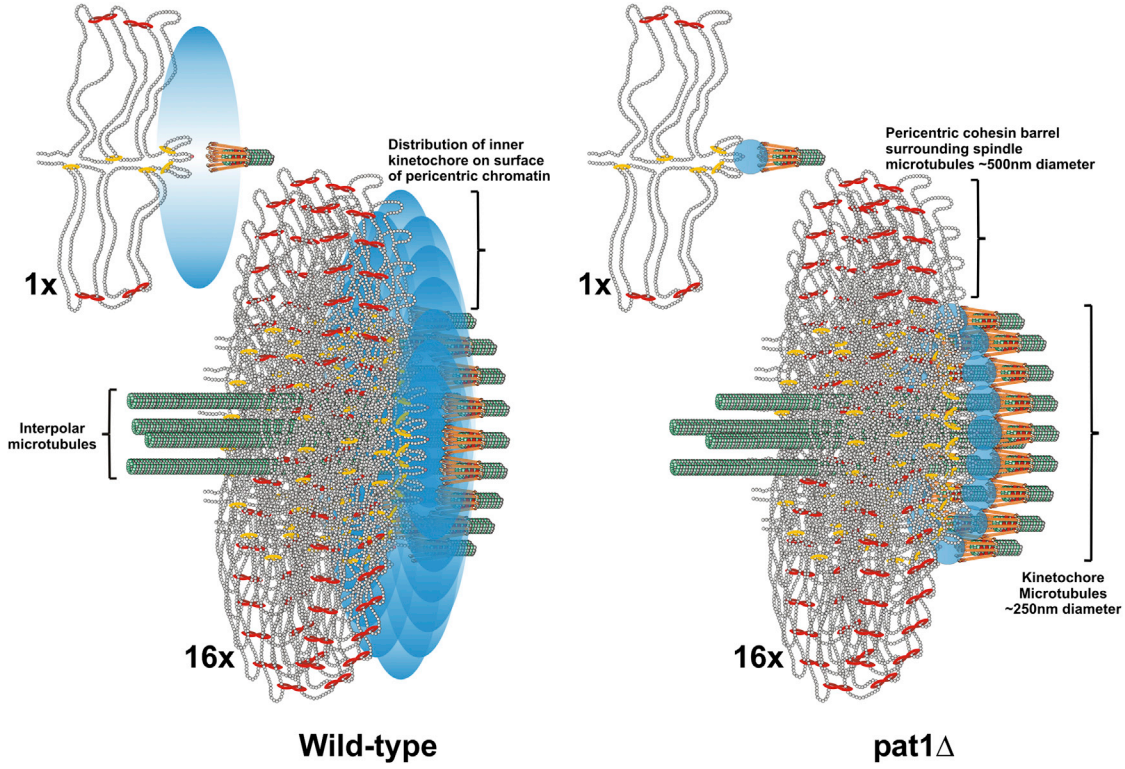

Figure 4. The Inner Kinetochore Is Organized into a Disc at the Surface of the Pericentric Chromatin in Mitosis

The pericentromere DNA is organized as a network of loops with the centromere DNA at the apex (DNA strands shown as strings of nucleosomes in gray) [11–13]. The centromere is attached to microtubule plus-ends via the kinetochore (orange barbells surrounding the microtubule in green). Cohesin (red) and condensin (yellow) are enriched in the pericentromere and surround the central spindle [12, 13]. A single pericentric region (one sister) is shown (1X). In metaphase centromeres from the 16 chromosomes are clustered around 16 kinetochore microtubules that emanate from the spindle pole body (16X, below). 4 interpolar microtubules extend to overlap with 4 interpolar from the opposite spindle pole body (not shown). Only the section of the pericentric barrel at the interface of the kinetochore microtubules is shown for clarity. In wild-type, a Cse4 molecule (pink ball) resides at the centromere DNA (apex of the loop; see 1X, wild-type). Accessory molecules (Pat1 dependent) are in the vicinity, represented as a probability bubble (graded blue oval) at the microtubule plus-end. The emergent spatial arrangement upon clustering of 16 kinetochores (16X) predicts the anisotropy and experimentally generated statistical maps. The width of the density map for a single Cse4 nucleosome at each CEN and 4 molecules with a probability bubble 550nm around the spindle is 190 ± 141nm (data not shown). This distribution is commensurate with the intensity measurements of deconvolved Cse4 images (Figure 3, inset). Wild-type density maps of Cse4 have a width of 181 ± 155nm (Figure 3). In *pat1*Δ mutants, the accessory molecules are absent, and the remaining Cse4 resides at the kinetochore microtubule plus-end (blue circles, *pat1*Δ). The predicted geometry in the *pat1*Δ matches the isotropy and experimentally generated statistical maps (Figure 2). This arrangement suggests that Cse4 and other inner kinetochore components constitute an inner plate at the chromatin, much like that observed in the trilaminar structure at the chromosome surface of a mammalian kinetochore.

Experimental Procedures

Image Analysis

Yeast cells containing spindle pole body proteins (Spc29-RFP) and kinetochore components (fused to GFP) were imaged on a Nikon TE2000, widefield, 100X 1.4 NA Orca II with MetaMorph software. Images were aligned in Matlab (2010b) by taking the brightest pixel for one spindle pole and rotating the spindle until the second spindle pole is horizontal to the first. Spindles are used with a length range of 1.4–1.6 microns. The position in Z is taken into account.

Once the spindle is aligned, the GFP spots are rotated to the same degree. We find the brightest pixel, and this is converted to a distance based on the pixel size (65 nm). Prior to taking a measurement, the offset (in x,y) is adjusted based on the measured offset using fluorescent beads to calibrate the instrument. The poles are set at 0, 0, and the measurements are taken relative to the pole. Absolute numbers are used to place all positions in one quadrant (+,+) relative to the spindle pole.

Deconvolution

Images (13 planes, 200 nm apart, unbinned) were deconvolved using Huygens Compute engine 4.1.0 (Scientific Volume Imaging), and background was subtracted using MetaMorph Imaging. Quantitative fluorescence intensity using the box within a box method for background subtraction was determined as previously described [2, 22].

Simulation of Spindle Pole and Kinetochore Images

The Matlab/Simulink model was run to produce an output file containing population measurements of spindle length and the lengths of 16 left and 16 right kinetochore microtubules (kMTs) [12]. This csv file of lengths was then converted to xml files using a Matlab code to build the geometric bipolar spindle by specifying the geometry of the kMT arrangement (250 nm diameter radial array; [23]). Spindle poles were labeled red and the 32 kMT plus ends (kinetochores) were labeled green in the simulation. Geometric spindle xml files were convolved with the point spread function of our microscope using Microscope Simulator 2.2.1 [12, 15] (http://cismm.cs.unc.edu/downloads/). Experimentally obtained background (offset), noise variation (Gaussian standard deviation of noise), and maximum intensity (gain) were used in simulations. Simulated images of kinetochore clusters were analyzed in the same manner as experimentally acquired images to produce position probability density maps.

Please see the Supplemental Experimental Procedures for a table of strains used in this study.

Supplemental Information

Supplemental Information includes Supplemental Experimental Procedures, four figures, and two tables and can be found with this article online at http://dx.doi.org/10.1016/j.cub.2013.07.083.

Acknowledgments

We thank the members of the Bloom laboratory as well as the centromere community for productive and open scientific discourse. This work was supported by NIH R37 GM32238 (to K.B.) and NIH P41 EB002025 (to R.M.T. II; Center for Computer Integrated Systems for Microscopy and Manipulation). Support for M.A.B. and P.K.M. was provided by the Intramural Research Program of the National Cancer Institute, National Institutes of Health.

Received: April 3, 2013
Revised: June 28, 2013
Accepted: July 30, 2013
Published: September 26, 2013

References

1. Joglekar, A.P., Bloom, K., and Salmon, E.D. (2009). In vivo protein architecture of the eukaryotic kinetochore with nanometer scale accuracy. Curr. Biol. *19*, 694–699.
2. Haase, J., Stephens, A., Verdaasdonk, J., Yeh, E., and Bloom, K. (2012). Bub1 kinase and Sgo1 modulate pericentric chromatin in response to altered microtubule dynamics. Curr. Biol. *22*, 471–481.
3. Mishra, P.K., Ottmann, A.R., and Basrai, M.A. (2013). Structural integrity of centromeric chromatin and faithful chromosome segregation requires Pat1. Genetics. Published online July 26, 2013. http://dx.doi.org/10.1534/genetics.113.155291.
4. Nissan, T., Rajyaguru, P., She, M., Song, H., and Parker, R. (2010). Decapping activators in Saccharomyces cerevisiae act by multiple mechanisms. Mol. Cell *39*, 773–783.
5. Swisher, K.D., and Parker, R. (2011). Interactions between Upf1 and the decapping factors Edc3 and Pat1 in Saccharomyces cerevisiae. PLoS ONE *6*, e26547.
6. Coffman, V.C., Wu, P., Parthun, M.R., and Wu, J.Q. (2011). CENP-A exceeds microtubule attachment sites in centromere clusters of both budding and fission yeast. J. Cell Biol. *195*, 563–572.
7. Lawrimore, J., Bloom, K.S., and Salmon, E.D. (2011). Point centromeres contain more than a single centromere-specific Cse4 (CENP-A) nucleosome. J. Cell Biol. *195*, 573–582.
8. Shivaraju, M., Unruh, J.R., Slaughter, B.D., Mattingly, M., Berman, J., and Gerton, J.L. (2012). Cell-cycle-coupled structural oscillation of centromeric nucleosomes in yeast. Cell *150*, 304–316.
9. Johnston, K., Joglekar, A., Hori, T., Suzuki, A., Fukagawa, T., and Salmon, E.D. (2010). Vertebrate kinetochore protein architecture: protein copy number. J. Cell Biol. *189*, 937–943.
10. Teixeira, D., and Parker, R. (2007). Analysis of P-body assembly in Saccharomyces cerevisiae. Mol. Biol. Cell *18*, 2274–2287.
11. Yeh, E., Haase, J., Paliulis, L.V., Joglekar, A., Bond, L., Bouck, D., Salmon, E.D., and Bloom, K.S. (2008). Pericentric chromatin is organized into an intramolecular loop in mitosis. Curr. Biol. *18*, 81–90.
12. Stephens, A.D., Haggerty, R.A., Vasquez, P.A., Vicci, L., Snider, C.E., Shi, F., Quammen, C., Mullins, C., Haase, J., Taylor, R.M., II., et al. (2013). Pericentric chromatin loops function as a non-linear spring in mitotic force balance. J. Cell Biol. *200*, 757–772.
13. Stephens, A.D., Haase, J., Vicci, L., Taylor, R.M., 2nd, and Bloom, K. (2011). Cohesin, condensin, and the intramolecular centromere loop together generate the mitotic chromatin spring. J. Cell Biol. *193*, 1167–1180.
14. Gonen, S., Akiyoshi, B., Iadanza, M.G., Shi, D., Duggan, N., Biggins, S., and Gonen, T. (2012). The structure of purified kinetochores reveals multiple microtubule-attachment sites. Nat. Struct. Mol. Biol. *19*, 925–929.
15. Quammen, C.W., Richardson, A.C., Haase, J., Harrison, B.D., Taylor, R.M., 2nd, and Bloom, K.S. (2008). FluoroSim: A Visual Problem-Solving Environment for Fluorescence Microscopy. Eurographics Workshop Vis. Comput. Biomed. *2008*, 151–158.
16. Santaguida, S., and Musacchio, A. (2009). The life and miracles of kinetochores. EMBO J. *28*, 2511–2531.
17. Verdaasdonk, J.S., Gardner, R., Stephens, A.D., Yeh, E., and Bloom, K. (2012). Tension-dependent nucleosome remodeling at the pericentromere in yeast. Mol. Biol. Cell *23*, 2560–2570.
18. Pearson, C.G., Yeh, E., Gardner, M., Odde, D., Salmon, E.D., and Bloom, K. (2004). Stable kinetochore-microtubule attachment constrains centromere positioning in metaphase. Curr. Biol. *14*, 1962–1967.
19. Gasser, S.M., Hediger, F., Taddei, A., Neumann, F.R., and Gartenberg, M.R. (2004). The function of telomere clustering in yeast: the circe effect. Cold Spring Harb. Symp. Quant. Biol. *69*, 327–337.
20. Jencks, W.P. (1975). Binding energy, specificity, and enzymic catalysis: the circe effect. Adv. Enzymol. Relat. Areas Mol. Biol. *43*, 219–410.
21. Henikoff, S., and Henikoff, J.G. (2012). "Point" centromeres of Saccharomyces harbor single centromere-specific nucleosomes. Genetics *190*, 1575–1577.
22. Hoffman, D.B., Pearson, C.G., Yen, T.J., Howell, B.J., and Salmon, E.D. (2001). Microtubule-dependent changes in assembly of microtubule motor proteins and mitotic spindle checkpoint proteins at PtK1 kinetochores. Mol. Biol. Cell *12*, 1995–2009.
23. Winey, M., and Bloom, K. (2012). Mitotic spindle form and function. Genetics *190*, 1197–1224.